Acta Crystallographica Section B
Structural Science
ISSN 0108-7681

Incommensurately modulated lanthanide coinage-metal diarsenides. II. $GdCuAs_2$, $GdAu_{1-\delta}As_2$ and $TbAu_{1-\delta}As_2$ – new distortion variants of the $HfCuSi_2$ type with irregularly stacked zigzag chains of arsenic atoms

D. Rutzinger, C. Bartsch, Th. Doert* and M. Ruck

Department of Chemistry and Food Chemistry, Technische Universität Dresden, D-01062 Dresden, Germany

Correspondence e-mail: thomas.doert@chemie.tu-dresden.de

Received 17 December 2008
Accepted 24 July 2009

$GdCuAs_2$, $GdAu_{1-\delta}As_2$ and $TbAu_{1-\delta}As_2$ crystallize as incommensurately modulated variants of the $HfCuSi_2$ type. Structure models have been developed in the monoclinic superspace group $P12_1/m1(\alpha0\gamma)00$ (No. 11.1). The components of the modulation wavevectors $\mathbf{q} = \alpha\mathbf{a}^* + 0\mathbf{b}^* + \gamma\mathbf{c}^*$ are $\alpha = 0.04$ (1) and $\gamma = 0.48$ (1) for $GdCuAs_2$, $\alpha = 0.03$ (1) and $\gamma = 0.48$ (1) for $GdAu_{1-\delta}As_2$ and $\alpha = 0.02$ (1) and $\gamma = 0.46$ (1) for $TbAu_{1-\delta}As_2$. The predominant effect of the positional modulation is the distortion of a square net of arsenic atoms, which results in planar zigzag chains. Rod groups and layer groups of the respective structure motifs are identified and discussed.

1. Introduction

Compounds with layered-type structures are the subject of intensive investigations owing to interesting structural features and physical properties. Among these compounds, $HfCuSi_2$-type lanthanide coinage metal diarsenides $LnTAs_2$ (Ln = Y, La, Ce–Lu; T = Cu, Ag, Au) exhibit local *Peierls*-like distortions in planar nets of arsenic atoms, which cause a reduction in symmetry (Mozharivskiy *et al.*, 2000, 2001; Demchyna *et al.*, 2004). Beside some distortion variants crystallizing as commensurate superstructures of the aristotype (Eschen & Jeitschko, 2003; Demchyna *et al.*, 2004), an incommensurately modulated structure with irregular stacking of planar *cis-trans* As chains has been discovered recently (Rutzinger *et al.*, 2009). During these X-ray studies, satellite reflections indicating incommensurate modulations have also been observed for $GdCuAs_2$, $GdAuAs_2$ and $TbAuAs_2$. The structure models developed for these three compounds are presented in the following.

2. Experimental

2.1. Synthesis

The starting materials were handled in an argon-filled glove box [M. Braun, $p(O_2) \leq 1$ p.p.m., $p(H_2O) \leq 1$ p.p.m., argon purification with molecular sieve and copper catalyst] in order to avoid reaction with air and moisture. Pieces of gadolinium (99.9%, ABCR) or terbium (99.9%, Acros) freshly filed from rods, copper (powder, p.a., Chemapol) or gold (powder, 99.9+%, Chempur GmbH) and arsenic (powder, > 99.997% metal-based, Aldrich; As_2O_3 removed by sublimation prior to use) were mixed in the atomic ratio of 1:1:2. The reactions were carried out in a sixfold excess of a LiCl/KCl flux (LiCl,

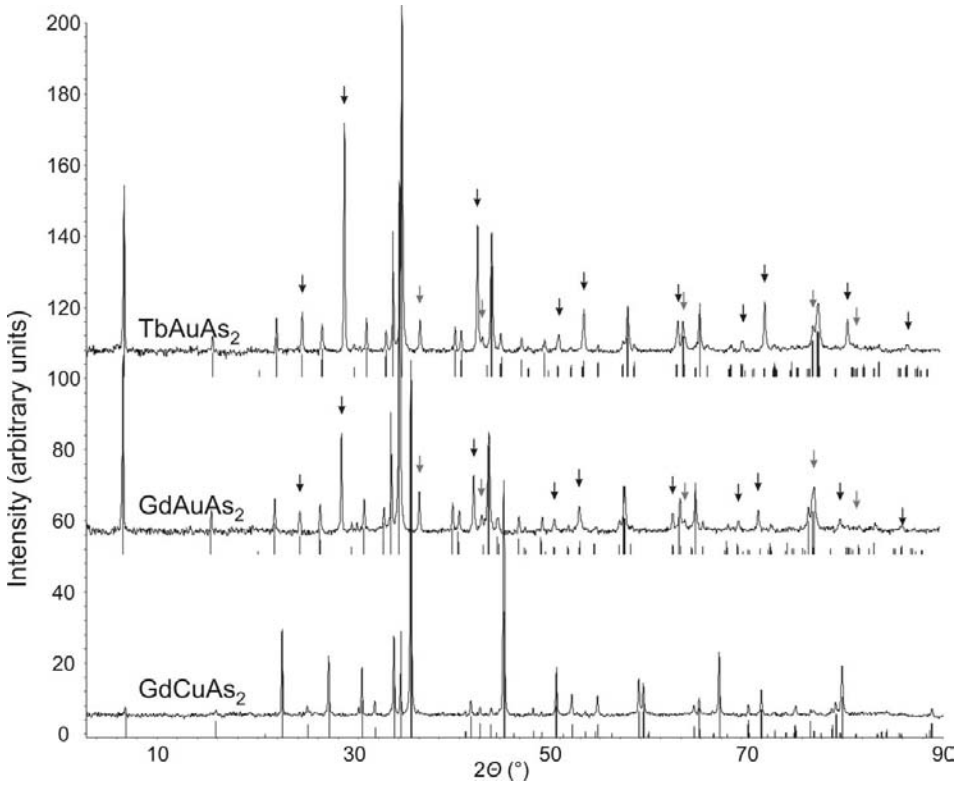

Figure 1
X-ray powder diffraction patterns of $TbAuAs_2$ (top), $GdAuAs_2$ (center) and $GdCuAs_2$ (bottom); reflections of the respective ternary compounds are indicated with black lines, reflections of by-products are highlighted (lanthanide arsenide black arrow, elemental gold gray arrow; *WinXPow*, Stoe & Cie, 1999).

KCl: powders, p.a, Merck, dried at 410 K in dynamic vacuum prior to use) in glassy carbon crucibles, which were sealed in evacuated silica tubes. The samples were heated to 1123 K within 48 h, annealed for 96 h, and cooled to 623 K over 192 h. The flux was removed with water and the products were washed with ethanol. Air-stable, shiny black platelets of the title compounds were obtained.

3. Results

Note that the title compounds were obtained with compositions $GdCuAs_2$, $GdAu_{0.973\,(3)}As_2$ and $TbAu_{0.966\,(3)}As_2$. To improve the readability in the text and in the figures, the two latter compounds are denoted as $GdAuAs_2$ and $TbAuAs_2$, respectively. In the crystallographic tables the actual compositions are given.

3.1. Powder pattern

Powder diffraction data of the reaction products (Fig. 1) revealed that only $GdCuAs_2$ was obtained as a single-phase sample under the conditions stated above. As can be seen from the diffractograms, $GdAuAs_2$ and $TbAuAs_2$ were accompanied by considerable amounts of the respective binary lanthanide arsenide LnAs and elemental gold at a reaction temperature of 1123 K. The reduction of the reaction temperature to 1023 K led to a lower but still detectable amount of the by-products. Crystals of the target compounds for X-ray investigations were selected manually.

3.2. Basic structure

Precession photographs of $GdCuAs_2$, $GdAuAs_2$ and $TbAuAs_2$ revealed a (pseudo-)tetragonal unit cell with $a \simeq b \simeq 4$ Å and $c \simeq 10$ Å. The satellite reflections were visible as blurred spots only. The monoclinic space group $P12_1/m1$ (No. 11) was deduced for the basic structures in accordance with lattice parameters and diffraction images (*see below*). The basic structures consist of PbO-like layers of planar nets of the coinage metal *T*, alternately capped by As1 atoms, and planar, nearly square nets of As2 atoms stacked along [001]. The Ln atoms occupy positions between these two building blocks. The basic structure of $TbAuAs_2$ in $P12_1/m1$ is shown in Fig. 2.

Each Ln atom is surrounded by a slightly distorted square antiprism of As1 atoms of the PbO-like layer and As2 atoms

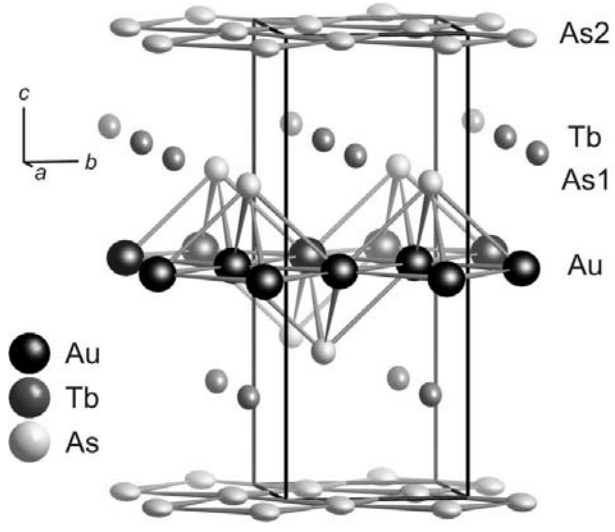

Figure 2
Basic structure of $TbAuAs_2$ in $P12_1/m1$ (No. 11), ellipsoids at the 99% probability level.

of the (nearly) square nets leading to four different Ln–As distances. The As1 atom is surrounded by a slightly distorted square antiprism of Ln and *T* atoms, the As2 atoms by four As2 atoms and four Ln atoms. The latter motif can be described as a (4 + 4) coordination set up by a compressed tetrahedron of Ln atoms and a square of As2 atoms around the central As2 atom (Fig. 3, left). The (4 + 4 + 4) coordination of the *T* atom consists of two interpenetrating elongated tetrahedra of Ln or As1 atoms and a rectangle with nearly equal sides of *T* atoms (Fig. 3, right). The quite large anisotropic displacement parameters of the As2 atoms can be taken as a hint of the modulation.

3.3. Modulated structure

Reciprocal layers, simulated from the diffractometer datasets, revealed satellites of low intensities for the three title compounds. Owing to the positions of these additional reflections and a constant splitting of their intensity maxima (*cf.* Fig. 4), commensurate superstructures and twinning of three-dimensional structures can be excluded as reasons for the additional reflections. As in the case of $CeAu_{1-\delta}As_2$ (Rutzinger *et al.*, 2009) we deal with incommensurate modulations here.

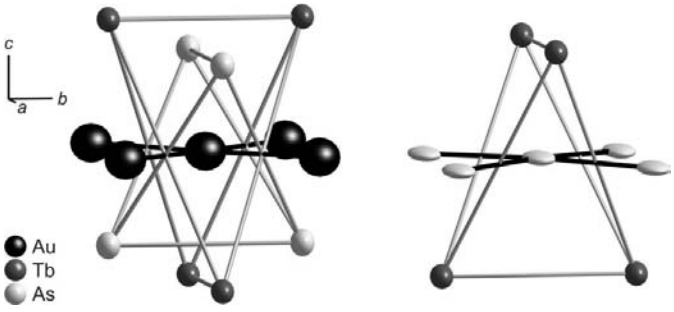

Figure 3
Coordination polyhedra of (*a*) the As2 atom and (*b*) the Au atom of $TbAuAs_2$ in the basic structure ($P12_1/m1$), ellipsoids at the 99% probability level.

Table 1
Twin laws and refined twin volume fractions of $GdCuAs_2$, $GdAuAs_2$ and $TbAuAs_2$.

Twin law	$GdCuAs_2$	$GdAuAs_2$	$TbAuAs_2$
$\begin{vmatrix} 1 & 0 & 0 \\ 0 & 1 & 0 \\ 0 & 0 & 1 \end{vmatrix}$	0.08 (2)	0.24 (1)	0.18 (2)
$\begin{vmatrix} 0 & \bar{1} & 0 \\ 1 & 0 & 0 \\ 0 & 0 & 1 \end{vmatrix}$	0.45 (1)	0.21 (1)	0.18 (1)
$\begin{vmatrix} \bar{1} & 0 & 0 \\ 0 & \bar{1} & 0 \\ 0 & 0 & 1 \end{vmatrix}$	0.10 (1)	0.36 (1)	0.33 (1)
$\begin{vmatrix} 0 & 1 & 0 \\ \bar{1} & 0 & 0 \\ 0 & 0 & 1 \end{vmatrix}$	0.36 (1)	0.19 (1)	0.31 (1)

The components of the modulation wavevectors $\mathbf{q} = \alpha\mathbf{a}^* + \beta\mathbf{b}^* + \gamma\mathbf{c}^*$ were determined to be $\alpha = 0.04$ (1) and $\gamma = 0.48$ (1) for $GdCuAs_2$, $\alpha = 0.03$ (1) and $\gamma = 0.48$ (1) for $GdAuAs_2$ and $\alpha = 0.02$ (1) and $\gamma = 0.46$ (1) for $TbAuAs_2$ with β being zero within 3σ in all cases (*X-Area*; Stoe & Cie, 2006; refinement of the **q** vectors without symmetry constraints).

A section of the reciprocal layer *h*2*l* of $TbAuAs_2$ recalculated from the recorded dataset is shown in Fig. 4(*a*). Looking at, for example, the area around the main reflection 020, two of the satellites can be attributed to the modulation vector **q** with $\alpha = 0.02$ (1) and $\gamma = 0.46$ (1) and $-\mathbf{q}$, respectively. These satellites, 0201 and $020\bar{1}$, are marked by red arrows. Obviously, two further satellites – indicated by blue arrows in the figure – are found around the main reflection 020, which can either be the result of a second modulation wavevector or of twinning of the crystal. As no cross terms, *i.e.* satellites attributed to the modulation vectors $\mathbf{q}_1 + \mathbf{q}_2$ and $\mathbf{q}_1 - \mathbf{q}_2$ with $\mathbf{q}_1 = (\alpha 0 \gamma)$ and $\mathbf{q}_2 = (-\alpha 0 \gamma)$ were detected, a two-dimensional modulation was excluded. Moreover, the section of the reciprocal layer *hk*0.46, depicted in Fig. 4(*b*), shows a pattern of four satellite maxima, one being *hklm* = 0201 again, emphasized by a black dot in the figure. This satellite pattern can only be the result of multiple twinning in the course of the symmetry reduction in accordance with the *Bärnighausen* graph presented in Fig. 5. The structure has hence been refined as a fourfold twin and the refined twin fractions are presented in Table 1. As can also be seen from Fig. 4, some of the main reflections show a

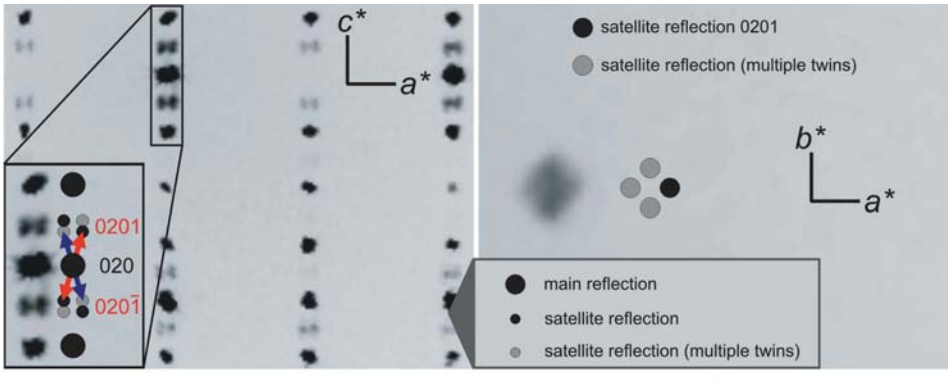

Figure 4
Satellite pattern in the diffraction image of $TbAuAs_2$: (*a*) area around main reflection 020 (section of the reciprocal layer *h*2*l*) and (*b*) satellite reflection 0201 with the contribution of twin individuals in a section of the reciprocal layer *hk*0.46.

Table 2
Wyckoff sites, occupancies, atomic coordinates, isotropic displacement parameters (Å^2) and Fourier coefficients of the positional modulation functions for $GdCuAs_2$, $GdAuAs_2$ and $TbAuAs_2$ in $P12_1/m1(\alpha 0\gamma)00$.

Atom	Site	Occupancy	x	y	z	U_{iso}	$x$sin 1	$z$sin 1	$x$cos 1	$z$cos 1
Gd	2*e*	1	0.2476 (3)	1/4	0.76146 (4)	0.0128 (1)	−0.0073 (2)	0.0005 (2)	0.0075 (2)	−0.0007 (2)
Cu	2*e*	1	0.744 (1)	1/4	0.4999 (2)	0.0166 (3)	−0.0139 (6)	0.0021 (5)	0.0004 (5)	0.0014 (6)
As1	2*e*	1	0.2543 (7)	1/4	0.34179 (8)	0.0134 (2)	−0.0098 (3)	0.00105 (4)	−0.0054 (3)	0.0008 (4)
As2	2*e*	1	0.740 (1)	1/4	0.9995 (2)	0.0175 (3)	0.0004 (5)	−0.0010 (4)	0.0261 (5)	−0.0039 (5)
Gd	2*e*	1	0.2519 (4)	1/4	0.76613 (5)	0.0129 (3)	0.0114 (3)	−0.0006 (3)	−0.0128 (3)	0.0004 (3)
Au	2*e*	0.973 (3)	0.7492 (4)	1/4	0.5006 (3)	0.0197 (3)	0.0217 (2)	−0.0024 (2)	0.0000 (3)	–0.0005 (2)
As1	2*e*	1	0.259 (1)	1/4	0.3123 (1)	0.0137 (6)	0.0146 (5)	−0.0006 (5)	0.0093 (5)	0.0002 (5)
As2	2*e*	1	0.751 (1)	1/4	0.9981 (6)	0.0188 (7)	0.0004 (6)	−0.0002 (5)	−0.0377 (7)	0.0032 (8)
Tb	2*e*	1	0.2494 (8)	1/4	0.76696 (6)	0.0179 (3)	0.0061 (4)	−0.0002 (3)	0.0066 (6)	0.0001 (3)
Au	2*e*	0.966 (6)	0.748 (1)	1/4	0.5007 (1)	0.0259 (3)	0.0121 (3)	−0.0014 (2)	0.0000 (3)	0.0009 (4)
As1	2*e*	1	0.267 (2)	1/4	0.3100 (1)	0.0174 (6)	0.0088 (8)	0.0017 (6)	0.0059 (8)	0.0013 (6)
As2	2*e*	1	0.751 (3)	1/4	0.9982 (4)	0.0246 (8)	0.0001 (8)	0.0002 (5)	−0.0218 (9)	−0.0004 (8)

$x$sin 1, $x$cos 1, $z$sin 1 and $z$cos 1 correspond to atomic displacement waves along x and z, respectively.

tendency to splitting. This can be taken as further evidence for the twinning.

Since the modulation wavevector $\mathbf{q} = \alpha\mathbf{a}^* + \beta\mathbf{b}^* + \gamma\mathbf{c}^*$ with the observed components $\alpha = 0.02\,(1)$ and $\gamma = 0.46\,(1)$ is incompatible with tetragonal or orthorhombic symmetry, the symmetry had to be reduced to the monoclinic crystal system. Owing to the reflection conditions for the satellites, the monoclinic superspace group $P12_1/m1(\alpha 0\gamma)00$ (No. 11.1; Janssen *et al.*, 2004) with $\beta = 90.0\,(3)^\circ$ was chosen for structure refinement. Based on the parent $HfCuSi_2$-type in the space group *P*4/*nmm* (No. 129) a three-dimensional model in this superspace group was developed following the *Bärnighausen* formalism stated in Fig. 5 (Bärnighausen, 1980; Wondratschek & Müller, 2006). Note that the same superspace-group symmetry has been found for the incommensurately modulated compound $CeAu_{1-\delta}As_2$ (Rutzinger *et al.*, 2009), although the two types of modulated structures differ substantially in their structural motifs. The reduction in symmetry *via* two *translationengleiche* steps of index 2 reflects the loss of the fourfold axis. Each of these *t*2 steps of symmetry reduction may give rise to the formation of twins and a fourfold twin is likely to result in the end.

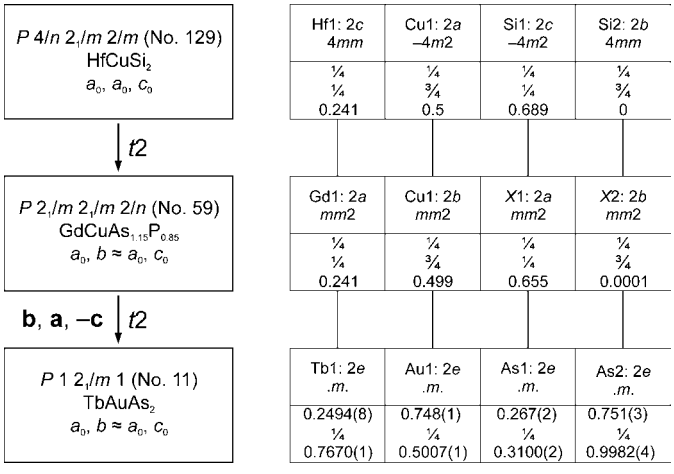

Figure 5
Bärnighausen tree for the symmetry relation between the $HfCuSi_2$ (*P*4/*nmm*) and the $TbAuAs_2$ structure ($P12_1/m1$). Note that the atomic positions of the $HfCuSi_2$ type are shifted by $z + \frac{1}{2}$ with respect to the data given in the original publication by Andrukhiv *et al.* (1975).

As observed for the commensurate superstructure of $PrAgAs_2$ (Eschen & Jeitschko, 2003), the displacement of the arsenic atoms of the planar nets was found to be the predominant effect of the modulation. One harmonic modulation wave for the positional modulation and for the displacement parameters of all atoms was introduced, higher modulation waves were not considered as only first-order satellites were observed in the diffraction data. The occupancy of the gold atoms was refined to 0.973 (3) for $GdAuAs_2$ and 0.966 (3) for $TbAuAs_2$, which led to a considerable drop in the *R* values. No occupancy modulation was observed. Note that the gold deficiency has no impact on the distortion since stoichiometric $GdCuAs_2$ crystallizes with the same structural motifs. Transition metal deficiency in $HfCuSi_2$ related structures has also been found for some antimonides (Cordier *et al.*, 1985; Ferguson *et al.*, 1996). The atomic parameters are listed in Table 2, final results of the refinements as well as relevant crystallographic data can be found in Table 3,[1] and interatomic distances are stated in Table 4.

The refined atomic modulation functions of $GdCuAs_2$ and $TbAuAs_2$ are displayed within the respective difference-Fourier ($F_o - F_c$) and Fourier (F_o) maps in Fig. 6. Only the x_1–x_4 maps are shown as the major impact of the positional modulations are visible here. The comparatively large displacement of the As2 atom along [100] results in the formation of zigzag chains with enlarged gaps between the chains. Overall, the electron-density distribution is modeled quite well by the calculated atomic modulation functions (left panels of Fig. 6) and the $F_o - F_c$ maps are balanced, although residual maxima and minima of up to 3.84 and −3.65 e Å^{-3}

[1] Supplementary data for this paper are available from the IUCr electronic archives (Reference: CK5036). Services for accessing these data are described at the back of the journal.

Table 3
Crystallographic and refinement data for $GdCuAs_2$, $GdAuAs_2$ and $TbAuAs_2$.

	(I)	(II)	(III)
Crystal data			
Chemical formula	$GdCuAs_2$	$GdAu_{0.973\,(3)}As_2$	$TbAu_{0.966\,(6)}As_2$
M_r	370.6	498.7	499.0
Crystal system, superspace group	Monoclinic, $P12_1/m1(\alpha0\gamma)00$ (No. 11.1)	Monoclinic, $P12_1/m1(\alpha0\gamma)00$ (No. 11.1)	Monoclinic, $P12_1/m1(\alpha0\gamma)00$ (No. 11.1)
Temperature (K)	293	293	293
a, b, c (Å)	3.9041 (8), 3.902 (1), 9.908 (2)	3.9570 (8), 4.060 (2), 10.135 (2)	3.933 (2), 4.089 (2), 10.135 (2)
β (°)	90.05 (3)	90.01 (3)	90.0 (3)
V (Å^3)	150.92 (5)	162.82 (9)	163.01 (12)
Modulation wavevector	$\mathbf{q} = \alpha\mathbf{a}^* + \beta\mathbf{b}^* + \gamma\mathbf{c}^*$	$\mathbf{q} = \alpha\mathbf{a}^* + \beta\mathbf{b}^* + \gamma\mathbf{c}^*$	$\mathbf{q} = \alpha\mathbf{a}^* + \beta\mathbf{b}^* + \gamma\mathbf{c}^*$
Wavevector component α	0.04 (1)	0.03 (1)	0.02 (1)
β	0	0	0
γ	0.48 (1)	0.48 (1)	0.46 (1)
Z	2	2	2
Radiation type	Mo $K\alpha$	Mo $K\alpha$	Mo $K\alpha$
μ (mm^{-1})	50.25	83.84	84.78
Crystal form, size (mm)	Platelet, 0.26 × 0.06 × 0.02	Platelet, 0.31 × 0.06 × 0.003	Platelet, 0.13 × 0.12 × 0.01
Laue class	$2/m$	$2/m$	$2/m$
Data collection			
Diffractometer	Stoe IPDS II	Stoe IPDS II	Stoe IPDS II
Sample detector distance (mm)	70	70	70
Data collection method	ω scans	ω scans	ω scans
Absorption correction	Numerical	Numerical	Numerical
T_{min}, T_{max}	0.128, 0.460	0.064, 0.807	0.066, 0.892
No. of measured, independent and observed reflections	10072, 2043, 751	9508, 2428, 1634	9845, 2101, 1091
Criterion for observed reflections	$I > 3\sigma(I)$	$I > 3\sigma(I)$	$I > 3\sigma(I)$
R_{int}, R_σ	0.066, 0.016	0.077, 0.022	0.059, 0.013
θ_{max}	34.1	33.8	33.4
No. of unique reflections (all/obs)	2056/764	2434/1640	2092/1083
No. of main reflections (all/obs)	666/543	1118/1039	686/642
No. of satellites (all/obs)	1390/221	1316/601	1406/441
Refinement			
Refinement on	F	F	F
Refined modulation wave	$1\cdot\mathbf{q}$	$1\cdot\mathbf{q}$	$1\cdot\mathbf{q}$
R_1, $wR_2(I > 3\sigma)$; R_1, wR_2 (overall)	0.039, 0.036; 0.104, 0.039	0.046, 0.049; 0.068, 0.050	0.055, 0.064; 0.088, 0.065
R_1, $wR_2(I > 3\sigma)$; R_1, wR_2 (all I) (main reflections)	0.033, 0.032; 0.040, 0.033	0.035, 0.039; 0.038, 0.039	0.050, 0.062; 0.053, 0.062
R_1, $wR_2(I > 3\sigma)$; R_1, wR_2, (all I) (satellites)	0.091, 0.092; 0.289, 0.113	0.104, 0.097; 0.187, 0.100	0.096, 0.096; 0.240, 0.110
S (all I)	1.24	2.37	2.96
No. of reflections	2043	2428	2101
No. of parameters	77	78	78
$(\Delta/\sigma)_{max}$	0.022	0.042	0.034
$\Delta\rho_{max}$, $\Delta\rho_{min}$ (e Å^{-3})	1.64, −1.97	3.04, −2.62	3.84, −3.65
Extinction method	B-C type 1 Gaussian isotropic (Becker & Coppens, 1974)	B-C type 1 Gaussian isotropic (Becker & Coppens, 1974)	B-C type 1 Gaussian isotropic (Becker & Coppens, 1974)
Extinction coefficient	0.14 (1)	0.19 (5)	0.26 (3)

Computer programs used: *X-Area* (Stoe & Cie, 2006), *SHELX*97 (Sheldrick, 2008), *JANA*2000 (Petříček *et al.*, 2000), *DIAMOND* (Brandenburg, 2001).

are found (in the case of $TbAuAs_2$). We believe that these are truncation effects as they appear to be more pronounced for the gold compounds. However, misfits may also arise from non-perfect absorption corrections and multiple twinning. The distortion within the As nets also influences the other atoms, as can be seen in the t plots for Ln, T and As1 (Fig. 7). The formation of the As2 zigzag chains leads to enlarged voids between the chains causing, in turn, a dislocation of the Ln atoms in the opposite direction along x_1. Transferred by the Ln atoms the As1 and T atoms of the PbO-like layers are shifted opposite As2 along x_1 (Fig. 7).

Choosing 2.828 Å as the upper limit to generate only bonded As2 atoms in $TbAuAs_2$, three different motifs can be identified: zigzag chains in *in-phase* or *anti-phase* orientations (*in-phase* orientation is defined as the orientation of the majority of the chains), and isolated As2 atoms on the border between *in-phase* and *anti-phase* chains. For these motifs rod groups were determined according to *International Tables for Crystallography* (Kopsky & Litvin, 2006). The propagation direction of the zigzag chains and consequently of the isolated As2 atoms is along [010]. Both zigzag chains and isolated As2 atoms possess monoclinic/rectangular symmetry, the zigzag

Table 4
Selected interatomic distances of $GdCuAs_2$, $GdAuAs_2$ and $TbAuAs_2$.

$GdCuAs_2$				$GdAu_{0.973\,(3)}As_2$				$TbAu_{0.966\,(6)}As_2$			
	Ave.	Min.	Max.		Ave.	Min.	Max.		Ave.	Min.	Max.
Gd—As1^{i,ii}	2.948 (3)	2.945 (3)	2.951 (3)	Gd—As1^{i,ii}	2.973 (4)	2.970 (4)	2.977(4)	Tb—As1^{i,ii}	2.985 (6)	2.974 (6)	2.996 (6)
Gd—As1^{iii,iv}	2.938 (3)	2.934 (3)	2.943 (3)	Gd—As1^{iii,iv}	2.915 (4)	2.908 (4)	2.922 (4)	Tb—As1^{iii,iv}	2.901 (6)	2.897 (6)	2.904 (6)
Gd—As2^{v}	3.082 (5)	3.017 (5)	3.145 (5)	Gd—As2^{v}	3.074 (8)	3.003 (9)	3.148 (9)	Tb—As2^{v}	3.06 (1)	3.03 (1)	3.08 (1)
Gd—As2	3.042 (5)	3.026 (5)	3.059 (5)	Gd—As2	3.071 (8)	3.038 (9)	3.104 (9)	Tb—As2	3.06 (1)	3.03 (1)	3.10 (1)
Gd—As2^{vi,vii}	3.070 (4)	3.037 (4)	3.107 (4)	Gd—As2^{vi,vii}	3.140 (8)	3.112 (8)	3.174 (8)	Tb—As2^{vi,vii}	3.139 (6)	3.135 (6)	3.141 (7)
Gd—Cu^{v}	3.253 (6)	3.239 (6)	3.268 (6)	Gd—Au^{v}	3.347 (4)	3.342 (4)	3.352 (4)	Tb—Au^{v}	3.341 (5)	3.333 (5)	3.349 (5)
Gd—Cu	3.236 (6)	3.213 (6)	3.260 (6)	Gd—Au	3.335 (4)	3.310 (4)	3.359 (4)	Tb—Au	3.337 (5)	3.319 (5)	3.354 (5)
Gd—Cu^{iii,iv}	3.242 (5)	3.228 (5)	3.255 (5)	Gd—Au^{iii,iv}	3.381 (4)	3.366 (4)	3.395 (4)	Tb—Au^{iii,iv}	3.397 (4)	3.385 (4)	3.409 (4)
Cu—Cu^{iii,iv}	2.726 (5)	2.724 (5)	2.728 (5)	Au—Au^{iii,iv}	2.830 (2)	2.824 (2)	2.836 (2)	Au—Au^{iii,iv}	2.829 (4)	2.826 (4)	2.831 (4)
Cu—Cu^{viii,ix}	2.794 (5)	2.787 (5)	2.801 (5)	Au—Au^{viii,ix}	2.839 (2)	2.834 (2)	2.844 (2)	Au—Au^{viii,ix}	2.845 (4)	2.843 (4)	2.848 (4)
Cu—As1	2.471 (7)	2.464 (7)	2.478 (7)	Au—As1	2.720 (6)	2.716 (6)	2.725 (6)	Au—As1	2.707 (8)	2.684 (8)	2.729 (8)
Cu—As1^{x}	2.535 (7)	2.521 (7)	2.548 (7)	Au—As1^{x}	2.777 (6)	2.750 (6)	2.804 (6)	Au—As1^{x}	2.809 (8)	2.779 (8)	2.839 (8)
Cu—As1^{iii,iv}	2.503 (5)	2.492 (5)	2.515 (5)	Au—As1^{iii,iv}	2.779 (5)	2.763 (5)	2.794 (5)	Au—As1^{iii,iv}	2.804 (5)	2.778 (5)	2.830 (5)
				As1—As2^{xi}	3.77 (1)	3.69 (1)	3.86 (1)	As1—As2^{xiii}	3.76 (1)	3.67 (1)	3.85 (1)
				As1—As2^{xii}	3.73 (1)	3.59 (1)	3.88 (1)	As1—As2^{xiv}	3.69 (1)	3.65 (1)	3.73 (1)
As2—As2^{vi,vii}	2.705 (5)	2.568 (4)	2.850 (5)	As2—As2^{vi,vii}	2.848 (5)	2.641 (5)	3.058 (6)	As2—As2^{vi,vii}	2.84 (1)	2.72 (1)	2.96 (1)
As2—As2^{xi,xii}	2.820 (5)	2.675 (5)	2.967 (5)	As2—As2^{xi,xii}	2.831 (5)	2.632 (5)	3.044 (6)	As2—As2^{xi,xii}	2.83 (1)	2.72 (1)	2.95 (1)

Symmetry codes: (i) $-x, -y, 1-z$; (ii) $-x, 1-y, 1-z$; (iii) $1-x, -y, 1-z$; (iv) $1-x, 1-y, 1-z$; (v) $-1+x, y, z$; (vi) $1-x, -y, 2-z$; (vii) $1-x, 1-y, 2-z$; (viii) $2-x, -y, 1-z$; (ix) $2-x, 1-y, 1-z$; (x) $1+x, y, z$; (xi) $2-x, -y, 2-z$; (xii) $2-x, 1-y, 2-z$; (xiii) $-1+x, y, -1+z$; (xiv) $x, y, -1+z$.

chains have $p12_1/m1$ symmetry (No. 12, left in Fig. 8), whereas the row of isolated atoms comprises $p12/m1$ symmetry (No. 11).

For $TbAuAs_2$ the As2—As2 intrachain distances vary between 2.719 (6) and 2.828 (1) Å as a result of the positional modulation. The chain motifs can be grouped in two blocks of different length along [100]: blocks of the majority case contain 26 *in-phase* chains of the same orientation (purple in Fig. 9), whereas those of the minority case contain 23 chains with an *anti-phase* orientation (shift by $\Delta y = 0.5$, green) with respect to those of the majority blocks. The different blocks are, owing to the modulation, alternately arranged and separated by isolated As2 atoms. This centrosymmetric arrangement, hereafter denoted as layer, spreads over 50 basic units cells along [100] and exhibits orthorhombic layer-group symmetry $p2/b2_1/m2/m$ (No. 40, Fig. 9). The stacking sequence

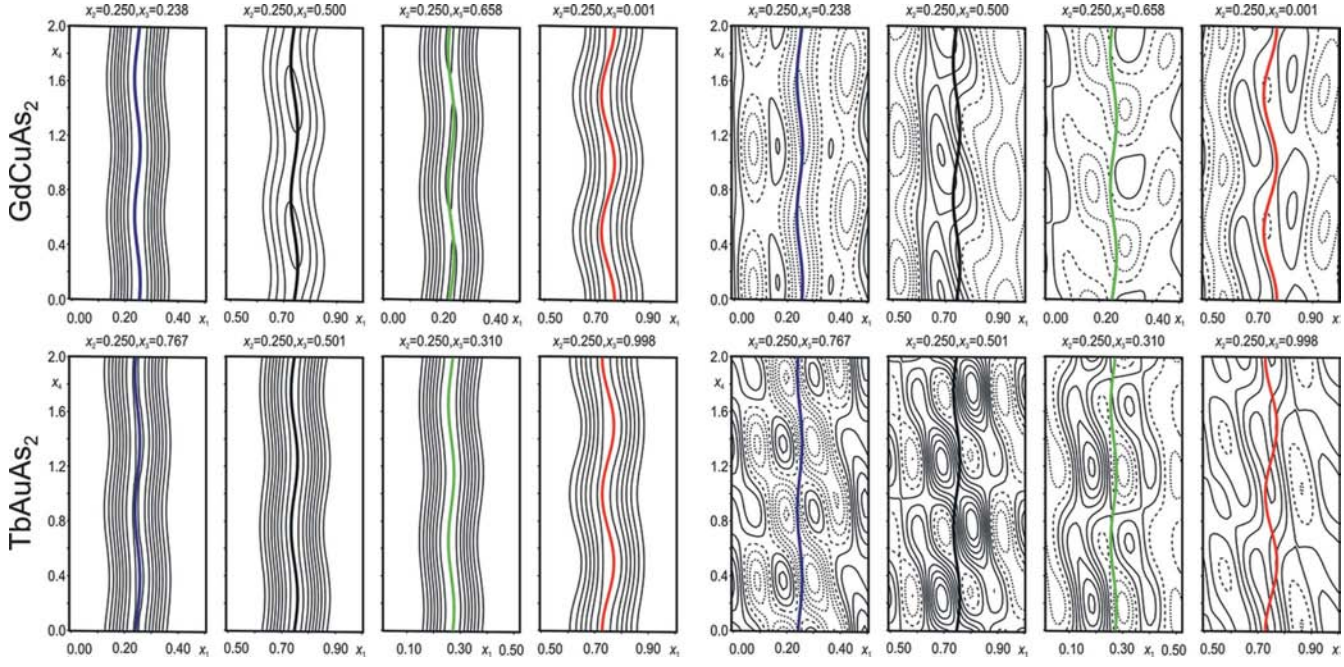

Figure 6
Fourier maps and difference-Fourier maps for $GdCuAs_2$ (top) and $TbAuAs_2$ (bottom); bold lines: calculated atom modulation functions for Gd, Tb (blue), Cu, Au (black), As1 (green) and As2 (red); steps of electron densities 40 e Å^{-3} per line for Gd, Tb, Au, 20 e Å^{-3} per line for Cu, As in the Fourier maps, 0.25 e Å^{-3} per line in the difference-Fourier maps of $GdCuAs_2$ and 0.5 e Å^{-3} per line in the difference-Fourier maps of $TbAuAs_2$.

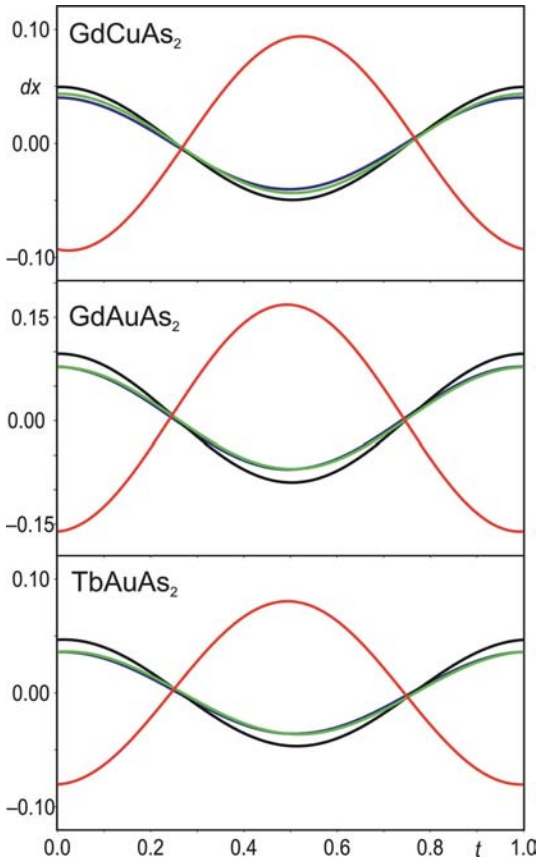

Figure 7
t plots of the positional modulations (lanthanide metals: blue lines, coinage metals: black lines, As1: green lines, As2: red lines) along **a** for $GdCuAs_2$ (top), $GdAuAs_2$ (center) and $TbAuAs_2$ (bottom).

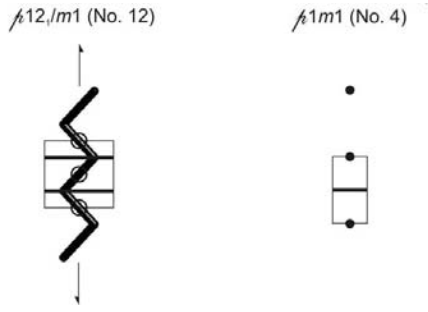

Figure 8
Rod groups of the different motifs: zigzag chains in rod group $p12_1/m1$ (No. 12, left) and isolated atoms in rod group $p12/m1$ (No. 11, right), both monoclinic/rectangular.

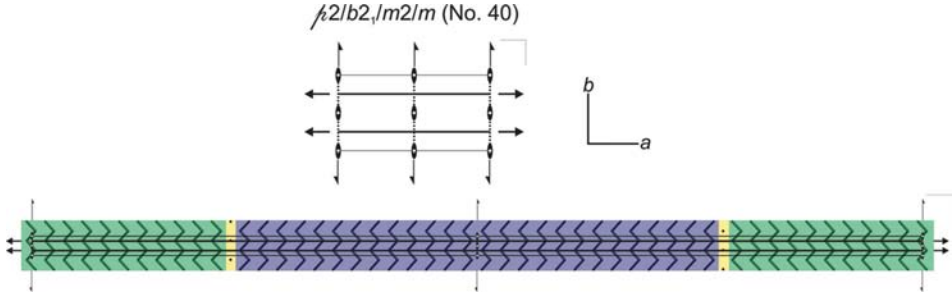

Figure 9
Top: sketch of layer group $p2/b2_1/m2/m$ (No. 40); bottom: layer group $p2/b2_1/m2/m$ applied to the modulated As net of $TbAuAs_2$.

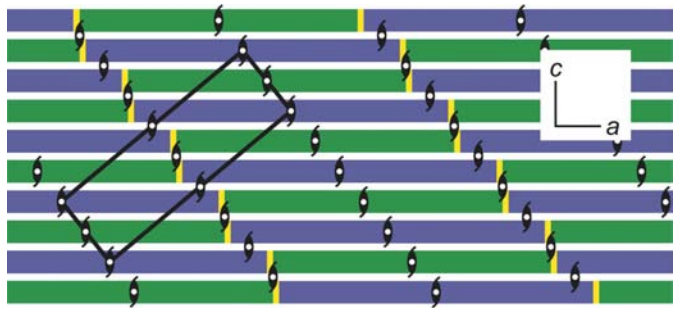

Figure 10
Stacking of layers of the modulated As nets of $TbAuAs_2$ along [001], color code according to Fig. 10. The positions of the twofold screw axes are highlighted, the repetition unit ($a' = 25.66$, $b' = 4.089$, $c' = 77.78$ Å, $\beta' = 92.84^\circ$) is emphasized with bold black lines.

of the layers along [001] is realised with an offset of $\Delta a = 23$ basic unit cells and results in the pattern displayed in Fig. 10. This pattern reveals the monoclinic symmetry of the space group $P12_1/m1$. The complete pattern can be tiled with a repetition unit of $a' = 25.66$, $b' = 4.089$, $c' = 77.78$ Å and $\beta' = 92.84^\circ$ (indicated by black lines in Fig. 10) which can be obtained by the transformation matrix (40 1 5, 0 1 0, −2 0 5) from the basic unit cell. Note that only the As net is discussed here and that the repetition unit is not an approximant of the entire modulated structure.

The modulation of $GdCuAs_2$ (Fig. 11) is more difficult to describe since blocks of different widths with the same orientation are found. The As2—As2 intra-chain distances vary between 2.568 (4) and 2.751 (8) Å here. Choosing 2.751 Å as the upper limit for bonded As2, the chains are grouped into four blocks of different width and orientation always separated by isolated As2 atoms. Two different sequences (layers) can be identified which cover 28 basic unit cells along *a*. This is achieved by the combination of a block consisting of 16 *in-phase* chains (purple in Fig. 11) and a block formed by 11 *anti-phase* chains (green) separated by isolated As2 atoms (yellow, layer A), or the combination of a block consisting of 15 *in-phase* chains (blue) and a block set up of 12 *anti-phase* chains (red) separated by isolated As2 atoms (layer B). Both layers exhibit orthorhombic layer-group symmetry $p2/b2_1/m2/m$ (No. 40, Fig. 11).

For $GdAuAs_2$, the As2—As2 intra-chain distances vary between 2.632 (5) and 2.822 (2) Å. The same blocks as in $GdCuAs_2$ are observed, however, grouped into one single type of layer which covers 100 basic unit cells along [100]. The layer group is $p2/b2_1/m2/m$ (No. 40, *cf.* Fig. 12) again.

The stacking of the layers of $GdCuAs_2$ and $GdAuAs_2$ along [001] results in the patterns shown in Figs. 13 and 14. For both, the monoclinic repetition unit compatible with space-group symmetry $P12_1/m1$ can be sketched (empha-

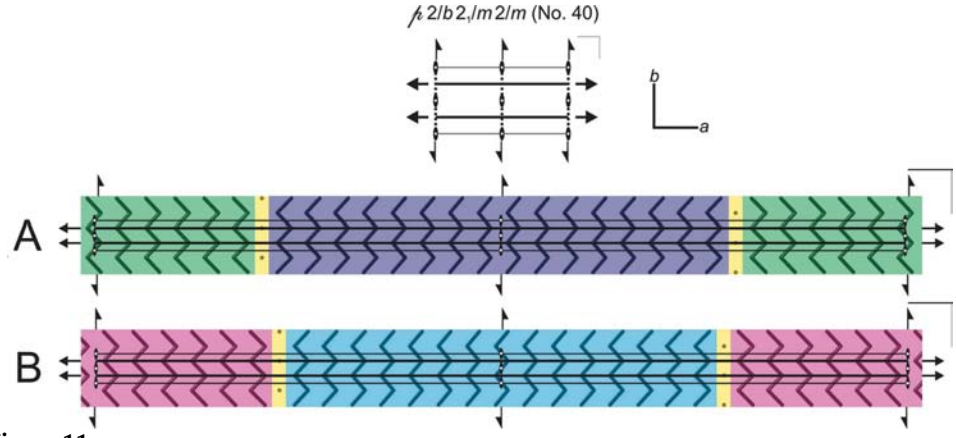

Figure 11
Sketches of the layer group $p2/b2_1/m2/m$ (No. 40) applied to the two different layers of $GdCuAs_2$. Top: layer A consisting of 16 *in-phase* chains and 11 *anti-phase* chains; bottom: layer B containing 15 *in-phase* chains and 12 *anti-phase* chains.

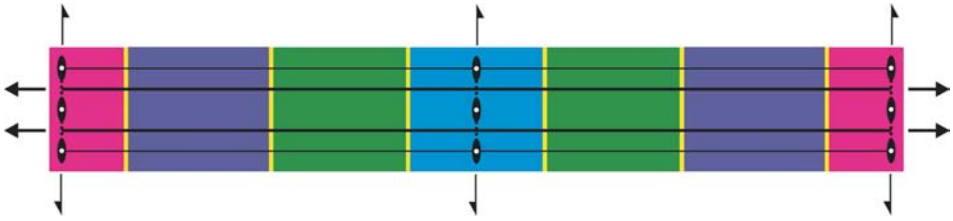

Figure 12
Layer group $p2/b2_1/m2/m$ (No. 40) applied to the layer of $GdAuAs_2$. For an explanation of the blocks, see text.

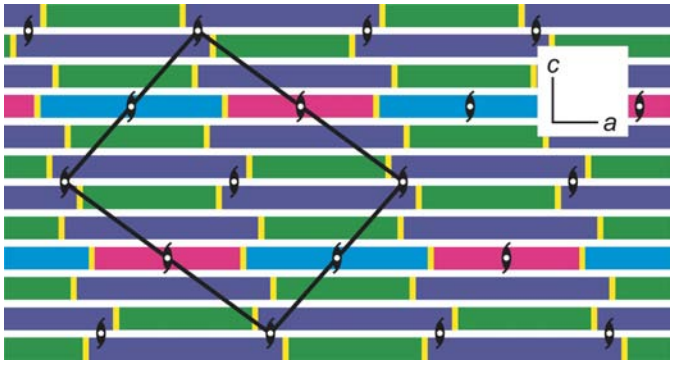

Figure 13
Stacking of the two different layers A and B of $GdCuAs_2$ along [001], color code according to Fig. 11. The positions of the twofold screw axes are highlighted, the monoclinic repetition unit with $a' = 65.56$, $b' = 3.9016$, $c' = 82.82$ Å, $\beta' = 94.18°$ is emphasized with bold black lines.

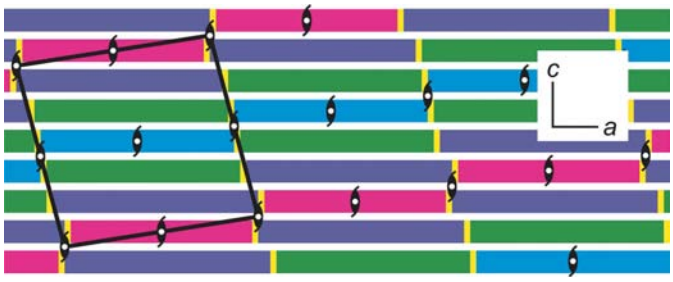

Figure 14
Stacking of the layer of modulated As nets of $GdAuAs_2$ along [001], color code according to Fig. 12. The positions of the twofold screw axes are highlighted, the monoclinic repetition unit with $a' = 62.84$, $b' = 4.060$, $c' = 64.12$ Å, $\beta' = 95.49°$ is emphasized with bold black lines.

sized by black lines in the figures). The repetition units have the dimensions $a' = 65.56$, $b' = 3.9016$, $c' = 82.82$ Å and $\beta' = 94.18°$ for $GdCuAs_2$ and $a' = 62.84$, $b' = 4.060$, $c' = 64.12$ Å and $\beta' = 95.49°$ for $GdAuAs_2$ and are linked to the basic unit cells by the transformation matrices (11 0 17, 0 1 0, 5 0 5) and (−4 0 16, 0 1 0, 6 0 1).

Financial support of Deutsche Forschungsgemeinschaft (Sonderforschungsbereich 463) is gratefully acknowledged.

References

Andrukhiv, L. S., Lysenko, L. A., Yarmolynuk, Ya. P. & Gladyshevskii, E. I. (1975). *Dopov. Akad. Nauk Ukr. RSR Ser. A*, pp. 645–648.

Bärnighausen, H. (1980). *Match*, **9**, 139–175.

Becker, P. J. & Coppens, P. (1974). *Acta Cryst.* A**30**, 129–147.

Brandenburg, K. (2001). *DIAMOND*, Version 2.1e. Crystal Impact GbR, Bonn, Germany.

Cordier, G., Schäfer, H. & Woll, P. (1985). *Z. Naturforsch. B*, **40**, 1097–1099.

Demchyna, R., Jemetio, J. P. F., Prots, Yu., Doert, Th., Akselrud, L. G., Schnelle, W., Kuz'ma, Yu. B. & Grin, Yu. (2004). *Z. Anorg. Allg. Chem.* **630**, 635–641.

Eschen, M. & Jeitschko, W. (2003). *Z. Naturforsch. B*, **58**, 399–409.

Ferguson, M. J., Hushagen, R. W. & Mar, A. (1996). *Inorg. Chem.* **35**, 4505–4512.

Janssen, T., Janner, A., Looijenga-Vos, A., de Wolff, P. M. & Prince, E. (2004). *International Tables for Crystallography*, Vol. C, ch. 9.8. Dordrecht: Kluwer Academic Publishers.

Kopsky, V. & Litvin, D. B. (2006). Editors. *International Tables for Crystallography*, Vol. E, *Subperiodic groups*, 1st online ed. Chester: International Union of Crystallography [doi:10.1107/97809553502060000105].

Mozharivskiy, Yu., Kaczorowski, D. & Franzen, H. F. (2000). *J. Solid State Chem.* **155**, 259–272.

Mozharivskiy, Yu., Kaczorowski, D. & Franzen, H. F. (2001). *Z. Anorg. Allg. Chem.* **627**, 2163–2172.

Petříček, V., Dušek, N. & Palatinus, L. (2000). *JANA*2000. Institute of Physics, Prague, Czech Republic.

Rutzinger, D., Doert, Th. & Ruck, M. (2009). *Acta Cryst.* B**65**, 519–526.

Sheldrick, G. M. (2008). *Acta Cryst.* A**64**, 112–122.

Stoe & Cie (1999). *WinXPow*. Stoe & Cie GmbH, Darmstadt, Germany.

Stoe & Cie (2006). *X-Area, IPDS 2 Software Package*. Stoe and Cie GmbH, Darmstadt.

Wondratschek, H. & Müller, U. (2006). Editors. *International Tables for Crystallography*, Vol. A1, 1st. ed. Dordrecht: Kluwer Academic Publishers.